PHYSICAL REVIEW D **94,** 114503 (2016)

Two-dimensional O(3) model at nonzero density: From dual lattice simulations to repulsive bosons

Falk Bruckmann,[1] Christof Gattringer,[2] Thomas Kloiber,[1,2] and Tin Sulejmanpasic[3]

[1]*Universität Regensburg, Institut für Physik, Universitätstraße 31, 93053 Regensburg, Germany*
[2]*Universität Graz, Institut für Physik, Universitätsplatz 5, 8010 Graz, Austria*
[3]*North Carolina State University, Department of Physics, Raleigh, North Carolina 27695-8202, USA*
(Received 12 August 2016; published 2 December 2016)

We discuss the thermodynamics of the O(3) nonlinear sigma model in $1+1$ dimensions at nonzero chemical potential (equivalent to a magnetic field). In its conventional field theory representation the model suffers from a sign problem. By dualizing the model, we are able to fully access the nonzero density regime of an asymptotically free theory with dynamical mass gap at arbitrary chemical potential values. We find a quantum phase transition at zero temperature where as a function of the chemical potential the density assumes a nonzero value. Measuring the spin stiffness we present evidence for a corresponding dynamical critical exponent z close to 2. The low energy O(3) model is conjectured to be described by a massive boson triplet with repulsive interactions. We confirm the universal square-root behavior expected for such a system at low density (and temperature) and compare our data to the results of Bethe *Ansatz* solutions of the relativistic and nonrelativistic one-dimensional Bose gas. We also comment on a potential Berezinskii-Kosterlitz-Thouless transition at nonzero density.

DOI: 10.1103/PhysRevD.94.114503

I. INTRODUCTION

Analyzing quantum field theories at nonzero temperature and chemical potential is of interest not only for studying their thermodynamical properties, but also for providing deep insights into the physical structure of the theory under consideration. A recent such example is given in [1], where we demonstrated that the grand canonical ensemble at low temperature and small volumes can be connected to scattering data.

Before we outline the physics results presented in this paper, we briefly mention the challenges of thermodynamics for numerical lattice simulations, one of our best *ab initio* tools (since analytic approaches are typically limited). Monte Carlo simulations are based on importance sampling and, while finite temperature simulations are routine, simulations at nonzero chemical potentials μ are in many cases plagued by the complex action/sign problem: at nonzero μ the action S has a nonvanishing imaginary part and the Boltzmann factor e^{-S} cannot be used as a probability weight in a stochastic process. One of the most successful methods is to employ dualization of the lattice path integral to new, so-called "dual variables," where the partition sum has only real and positive contributions (see, e.g., [2,3] for reviews). Although it is not completely clear for which classes of models a dual representation is useful for treating the sign problem, in models where it is successful the dual representation has allowed the exploration of the finite density phase diagrams, and the corresponding data also serve as a benchmark for other approaches to the complex action problem.

We would like to stress that dual representations not only enable simulations at nonzero density, but also reveal physical aspects complementary to those of the standard representation. In the dual representation the dynamical degrees of freedom are worldlines and the chemical potential couples to their temporal component. Via a discrete version of current conservation on a space-time lattice one finds that the chemical potential indeed couples to the temporal winding number of the worldlines. Thus the net number of particles (charged under the Noether charge of the corresponding symmetry) can be identified with the temporal net winding number of the worldlines and the Noether charge becomes topologically conserved. As such the worldlines winding around the time direction have a direct interpretation as quantum states carrying the corresponding quantum number. Since this is an all-scale statement, the dual worldlines carry direct information about the infrared physics, generally obscured in the conventional formulation of asymptotically free theories.

The O(3) nonlinear sigma model, which we are dealing with in this work, is conjectured to possess a particle triplet as its infrared excitations, the mass of which is generated dynamically. The dual wave function method of [1] indeed utilizes the spatial distance of the worldlines to obtain information about the particles' scattering. In the case of quantum chromodynamics (QCD), which is also asymptotically free, the low energy excitations are not the colored quarks and gluons, but colorless hadrons, with a large fraction of their masses being dynamically generated. A related dual lattice representation is that in terms of meson hoppings plus (anti-)baryon worldlines, to which the baryon chemical potential couples [4,5] (this dual representation, however, does not remove the sign problem completely and does not take into account the gauge action).

To be more concrete, we introduce a chemical potential for an O(2) subgroup of the O(3) symmetry of the sigma model in two dimensions. At low temperatures a nonzero density is expected to be induced into the system when μ reaches the threshold of the particle mass. In the condensed matter context μ can be viewed as a constant magnetic field inducing a magnetization; see Secs. 11 and 19 of [6]. We will analyze this transition in detail extending our previous simulations to large volumes. Beyond the transition the system explicitly breaks the global internal symmetry from $O(3)$ to $O(2)$ and in principle allows classical vortex solutions with half-integer topological charge [7]. Although at asymptotically large densities vortices are expected to bind in neutral pairs, it was conjectured in [7] that these vortices will be liberated at small densities, so that a Berezinskii-Kosterlitz-Thouless (BKT) transition [8,9] may happen at some finite value of the density. We remark that lattice results for the O(2) model at finite density can be found in [10–12].

Our main findings are twofold: Concerning the O(3) phase diagram we find a threshold *crossover* at nonzero temperatures and a *quantum phase transition* at zero temperature, as a function of μ at the mass threshold. Note that lattice simulations become expensive in this limit, as both temporal and spatial extensions must be taken to infinity. Using the concept of spin stiffness we analyze spatial correlations and present evidence for a dynamical critical exponent z close to 2, which is consistent with the nonrelativistic free fermions to which a model at low density belongs. We do not directly see signatures of a BKT transition conjectured in [7] in any of the observables studied in this work.

Secondly, the numerical data for the density near the transition can be described by a square root. The latter is universal for *one-dimensional repulsive bosons*. The simplest example of this is the nonrelativistic quantum particle gas with repulsive delta-function interactions (the Lieb-Liniger model [13]) and its limit when the repulsion strength goes to infinity (the Tonks-Girardeau limit [14,15]). The latter is equivalent to free fermions. These systems only differ in the specific form of the phase shifts, relevant away from the transition. Eigenstates and thermodynamics [16] of these systems can be obtained from Bethe *Ansätze*. We show that our data match well with the corresponding analytical nonrelativistic or relativistic predictions. Our simulations are performed at a lattice coupling in the continuum scaling regime, and we believe that the continuum limit to be performed does not reveal new qualitative features.

Our study demonstrates that dual lattice simulations are capable of describing a system all the way from the Lagrangian in terms of ultraviolet fields to the infrared physics in terms of interacting particles (at nonzero densities induced by μ). Such a transformation is the essence of Wilson's renormalization group, which is probably very hard to tackle analytically, but specific questions can be answered by the lattice, now that we have reliable lattice simulations at hand. To better understand the structure of dual partition functions and observables should also be of help in this program.

We briefly mention at the end that, although this program is mostly inspired by the attempts to understand the nonzero density structure of QCD, the potential benefit of studying nonlinear sigma models goes beyond this problem. Firstly, they are interesting in themselves and appear as effective models of (anti-)ferromagnetic systems. Secondly, the study of properties of these systems is interesting in the context of continuum quantum field theories themselves. On the one hand, we have recently shown for the example of the O(3) nonlinear sigma model that lattice dualities may provide a physical connection with the low energy excitations of the theory. On the other hand, the nonlinear sigma models play a crucial role in the development of the continuum definition of quantum field theories via the resurgence program (see [17] and references therein). To date, resurgent constructions were explicitly shown to work only in analytical tractable one-dimensional reductions of the O(N) [18] and CP(N) [19] nonlinear sigma models as well as of the principle chiral model [20]. However, genuinely $1+1$-dimensional nonzero density systems, akin to what we study here, also show similar resurgence structures [21]. Numerical and physical understanding of these systems is therefore important for the fundamentals of quantum field theory as well.

II. DEFINITION OF THE MODEL AND ITS LATTICE DISCRETIZATION

A. Continuum formulation and observables

The O(3) model is conventionally written in terms of normalized vectors $\vec{r}(x)=(r_1(x),r_2(x),r_3(x))$ with $\vec{r}(x)^2 = 1\ \forall\ x$ [also called "spins" or "O(3) rotors"] and the continuum action reads [22]

$$S[\vec{r}] = \frac{1}{g^2}\int d^2x \left[\frac{1}{2}(\partial_\nu r_a)^2 + i\mu(r_1\partial_2 r_2 - r_2\partial_2 r_1) + \frac{\mu^2}{2}r_3^2 - \frac{\mu^2}{2}\right], \tag{1}$$

where the coupling constant g is dimensionless in $1+1$ dimensions. We have already coupled a chemical potential μ to one of the O(2) subgroups, which excites the three-component of the angular momentum. Repeated indices are summed over (($\nu = 1, 2$) and ($a = 1, 2, 3$)) and arguments x have been dropped. At nonzero temperature T the Euclidean time x_2 is periodic with period $1/T$. In such a bosonic theory, μ also enters quadratically, tending to suppress the perpendicular component $r_3(x)$.

Our main thermodynamic observables will be the expectation values of the charge Q, its density n and its susceptibility χ_n:

$$Q = T\frac{\partial \ln Z}{\partial \mu}, \qquad n = \frac{Q}{L}, \qquad \chi_n = \frac{\partial n}{\partial \mu}, \tag{2}$$

where Z is the grand canonical partition function [see [23] or Eq. (12) below]. Eventually, all dimensionful quantities like μ, T, L, n etc. will be given in units of the mass m, e.g.,

$$\frac{n}{m} = \frac{T/m}{Lm}\frac{\partial \ln Z}{\partial(\mu/m)}, \tag{3}$$

whereas χ_n is already dimensionless.

We will also explore the spin stiffness for which one imposes twisted spatial boundary conditions for a finite spatial length L. To implement these, we first introduce the O(2) polar angle ϕ by combining the first two components into a complex number

$$r_1(x) + ir_2(x) = r_{12}(x)e^{i\phi(x)}, \tag{4}$$

and then replace the periodic boundary conditions in space by twisted ones,

$$\phi(x_1 + L, x_2) = \phi(x_1, x_2) + \varphi. \tag{5}$$

If the twist costs free energy, $F = -T\ln Z$, at leading order the dependence of F on φ is quadratic in φ, and we define the *spin stiffness* (also called superfluid density) by

$$\sigma = L\frac{\partial^2 F}{\partial \varphi^2}\bigg|_{\varphi=0} = -LT\frac{1}{Z}\frac{\partial^2 Z}{\partial \varphi^2}\bigg|_{\varphi=0}, \tag{6}$$

where we have used that Z is an even function of φ. Physically it is clear that σ depends on whether the regions x_1 and $x_1 + L$ are correlated, i.e., whether the system is in a (spatially) ordered state.

The spin stiffness can be computed and related to vortices in the lattice O(2) model without chemical potential[1] [24]. For large lattice coupling, the vortices are arranged in pairs and the spin correlator decays algebraically, which is the behavior closest to an ordered state in two dimensions (as the Mermin-Wagner theorem forbids the spontaneous breaking of the continuous symmetry). As a consequence, the spin stiffness σ will be nonzero. At small lattice coupling, the vortices condense and make the correlator decay exponentially. In this regime the spin stiffness σ will vanish if L is larger than the spatial correlation length ξ. This is why the spin stiffness can be used to detect BKT transitions characterized by the change of the correlator decay and to measure the spatial correlation length.

Actually, the dimensionful combination φ/L may be viewed as an imaginary chemical potential in the spatial direction, and therefore the stiffness is known to measure spatial winding numbers [25]. As this is best seen using dual variables, we give the corresponding formula in the next section.

B. Lattice formulation and the dual representation

The lattice action discretizing (1) reads

$$S[\vec{r}] = -J\sum_{\substack{x\in\Lambda\\ \nu=1,2}}\Big[r_3(x)r_3(x+\hat{\nu}) + \frac{1}{2}r_{12}(x)r_{12}(x+\hat{\nu}) \times \{e^{-i(\phi(x)-\phi(x+\hat{\nu}))-\mu\delta_{\nu,2}} + \text{c.c.}|_{\mu\to-\mu}\}\Big]. \tag{7}$$

As is common in lattice field theory, the chemical potential μ introduces exponential factors for the forward and backward temporal hopping terms. For $\mu = 0$ these terms are related by complex conjugation c.c., but when μ has a nonzero real part we face a complex action problem. The parameter J is the lattice coupling constant (dimensionless and positive) and the first sum runs over the $V \equiv N_s \times N_t$ sites of a two-dimensional lattice (Λ) with periodic boundary conditions. Again $\nu = 1, 2$ and $\hat{\nu}$ denotes the corresponding unit vector in direction ν. Throughout this paper we set the lattice spacing a to $a = 1$, implying that $T = 1/N_t$ and $L = N_s$.

The continuum limit for the lattice model is reached via $J \to \infty$. The mass gap of the system can be expressed in the bare coupling J and an UV cutoff as $m^2 = \Lambda_{\text{UV}}^2 \exp(-4\pi J)$. On the lattice the cutoff is proportional to the inverse lattice spacing, $\Lambda_{\text{UV}} = C/a$, and to two loops the mass gap reads [26,27]

$$am = C(1 + 2\pi J)\exp(-2\pi J) \quad \text{for } J \to \infty. \tag{8}$$

The partition sum is defined as the lattice path integral $Z = \int \mathcal{D}[\vec{r}]e^{-S[\vec{r}]}$, where the measure $\mathcal{D}[\vec{r}]$ is the product over the O(3)-invariant measures for $\vec{r}(x)$ on all lattice sites. The particle density and susceptibility are defined as μ-derivatives of Z as in the continuum,

$$n = \frac{1}{N_s N_t}\frac{\partial \ln Z}{\partial \mu}, \qquad \chi_n = \frac{\partial n}{\partial \mu}. \tag{9}$$

As a check we will also use the expectation value of the action density at $\mu = 0$,[2]

[1]The O(2) lattice action is $-J\sum_{x,\nu}\cos(\phi(x+\hat{\nu}) - \phi(x))$, which is nothing but (7) with $r_3 = 0$, $r_{12} = 1$ at $\mu = 0$.

[2]This is obtained from $e = \langle E\rangle/N_sN_t$, where $E = \sum_{x,\nu}(\nabla_\nu \vec{r})^2$ and $(\nabla_\nu f)(x) = f(x+\hat{\nu}) - f(x)$ [28]. From the normalization of $\vec{r}$ it follows that $e = 4 - 2\langle \vec{r}(x)\vec{r}(x+\hat{\nu})\rangle/N_sN_t$ and thus (10).

$$e = 4 - \frac{2}{N_s N_t}\frac{\partial \ln Z}{\partial J}, \tag{10}$$

whose strong and weak coupling expansions are [28]

$$e = \begin{cases} 4 - 4y - 8y^3 - \frac{48}{5}y^5 + \ldots, & \text{for small } J, \\ \frac{2}{J} + \frac{1}{4J^2} + \frac{0.156}{J^3} + \ldots & \text{for large } J, \end{cases} \tag{11}$$

where $y = \coth J - \frac{1}{J}$.

In [23] we have introduced the following (exact) representation of the partition function in terms of integer dual variables $m_{x,\nu} \in \mathbb{Z}$ and $k_{x,\nu}$, $\bar{m}_{x,\nu} \in \mathbb{N}_0$,

$$\begin{aligned} Z = \sum_{\{m,\bar{m},k\}} & \left(\prod_{x,\nu} \frac{J^{k_{x,\nu}}}{k_{x,\nu}!} \frac{(J/2)^{|m_{x,\nu}|+2\bar{m}_{x,\nu}}}{(|m_{x,\nu}| + \bar{m}_{x,\nu})!\bar{m}_{x,\nu}!} \right) e^{\mu \sum_x m_{x,2}} \\ & \times \prod_x \mathcal{I}\left(\sum_\nu (k_{x,\nu} + k_{x-\hat{\nu},\nu}), 1 + \sum_\nu [m_{x,\nu} + m_{x-\hat{\nu}} \right. \\ & \left. + 2(\bar{m}_{x,\nu} + \bar{m}_{x-\hat{\nu}})] \right) \\ & \times \prod_x \delta\left(\sum_\nu [m_{x,\nu} - m_{x-\hat{\nu},\nu}] \right) E\left(\sum_\nu [k_{x,\nu} + k_{x-\hat{\nu},\nu}] \right), \end{aligned} \tag{12}$$

where the Kronecker delta, the evenness function E and a function $\mathcal{I}$ related to Euler's beta function B have been used:

$$\delta(n) = \begin{cases} 1 & n = 0 \\ 0 & \text{else} \end{cases}, \qquad E(n) = \begin{cases} 1 & n \text{ even} \\ 0 & n \text{ odd} \end{cases},$$
$$\mathcal{I}(a,b) = B\left(\frac{a+1}{2}, \frac{b+1}{2}\right) = \frac{\Gamma(\frac{a+1}{2})\Gamma(\frac{b+1}{2})}{\Gamma(\frac{a+b+2}{2})}. \tag{13}$$

Note that the current $m_{x,\nu}$ is conserved since the Kronecker delta of $\sum_\nu [m_{x,\nu} - m_{x-\hat{\nu},\nu}] \equiv (\nabla m)_x$ corresponds to the discrete version of the vanishing divergence condition (at each site x). The chemical potential couples to the corresponding sum over the temporal components of $m_{x,\nu}$. This sum can be rewritten using the conservation as $\sum_x m_{x,2} = N_t \sum_{x_1} m_{x,2} = 1/T \cdot w[m]$, where $w[m]$ is the total winding number of the m-loops reflected in the net m-flux through every time slice. Thus, the chemical potential appears through weights $\exp(\mu \cdot \text{integer}/T)$. This is also the main advantage of dual representations of systems with respect to chemical potentials: if the dual partition function has no sign problem at vanishing μ, which holds for our system, μ does not introduce a sign problem either.

In the dual representation, the observables take the form

$$n = \frac{1}{N_s N_t}\left\langle \sum_x m_{x,2} \right\rangle = \frac{1}{N_s}\langle w[m] \rangle, \tag{14}$$

$$\chi_n = \frac{N_t}{N_s}(\langle w[m]^2 \rangle - \langle w[m] \rangle^2), \tag{15}$$

$$e = 4 - \frac{2}{N_s N_t}\left\langle \sum_{x,\nu} [k_{x,\nu} + |m|_{x,\nu} + 2\bar{m}_{x,\nu}] \right\rangle, \tag{16}$$

where here $\langle O \rangle$ is the expectation value of O in the dual representation obtained by inserting the expression O into the sum in Eq. (12) and dividing by Z.

We will also measure the space-time average of the third dual variable,

$$K = \frac{1}{N_s N_t}\left\langle \sum_{x,\nu} k_{x,\nu} \right\rangle, \tag{17}$$

as a measure for the anisotropy of the system. For its interpretation we sketch how the dual representation is obtained for the third variable, using that $Z \propto \int \mathcal{D}[\vec{r}] \prod_{x,\nu} \sum_{k_{x,\nu}=0}^{\infty} [J r_3(x) r_3(x+\hat{\nu})]^{k_{x,\nu}}/k_{x,\nu}!$. Evaluating (17) inserts another $k_{x,\nu}$ into the dual partition sum and reduces the argument of the factorial by 1, which can be compensated by a shift of the summation variable giving a factor of J and the hopping term. It follows that $\langle k_{x,\nu} \rangle = J \langle r_3(x) r_3(x+\hat{\nu}) \rangle$, where the latter expectation value is in the conventional representation (7). Hence K measures the amount of hopping in the direction perpendicular to the $x-y$ plane where we excite O(2) angular momentum. Thus, we expect K to be small in the anisotropic phase at large μ.

At vanishing μ the theory enjoys the full O(3) symmetry and the amount of hopping must be the same for all components. In the energy density (16) above this can be seen by virtue of the fact that $|m|_{x,\nu} + 2\bar{m}_{x,\nu}$ is the sum of two dual variables of the same nature as $k_{x,\nu}$; see Eq. (12) of [23]. Therefore, $e = 4 - 6K/J$ should hold at $\mu = 0$.

In the same way the chemical potential couples to the integrated temporal component of the conserved O(2) current, the twist-induced imaginary spatial chemical potential $i\varphi/L$ couples to the integrated spatial component. The partition function in the presence of the twist thus has an additional factor $\exp(i\varphi/N_s \cdot \sum_x m_{x,1}) = \exp(i\varphi w_s[m])$, where $w_s[m]$ is the total spatial winding number of m in each configuration. In the definition of the spin stiffness σ, Eq. (6), the second derivative with respect to φ brings down $-w_s[m]^2$ and setting φ to zero afterwards results in the expectation value

$$\sigma = \frac{N_s}{N_t}\langle w_s[m]^2 \rangle = LT \langle w_s[m]^2 \rangle, \tag{18}$$

in the dual representation without twist [similar to χ_n in Eq. (15)].

III. NUMERICAL SIMULATION, TESTS AND BASIC ANALYSIS

In this section we collect several more technical aspects of this paper. We briefly discuss our simulation strategy for the dual formulation and evaluate the correctness of its results by comparing them to perturbative strong and weak coupling calculations. Furthermore we present numerical results for the phase diagram at finite volume and temperature as well as a finite volume scaling analysis which indicates that at nonzero temperature all transitions are smooth crossovers.

A. Dual simulation and tests

In this subsection we briefly discuss Monte Carlo simulation strategies for the dual representation Eq. (12) and present tests for its correctness. Obviously each term in the partition sum (12) is real and positive and a probability interpretation of the weights of the dual configurations is possible. The remaining challenge of a dual Monte Carlo simulation is to generate only those configurations that obey all the constraints. For the unconstrained dual variables $\bar{m}_{x,\nu}$ conventional local Metropolis updates are sufficient. For the constrained variables $m_{x,\nu}$ and $k_{x,\nu}$ the constraints enforce closed loops and loops where flux is conserved modulo 2, respectively. In both cases one can generate new admissible configurations by changing the variables along an arbitrarily chosen closed loop which guarantees that the constraints remain intact. This loop along which one updates the dual variables can for example be grown in steps using local random choices and corresponding Metropolis decisions until it closes, which is the well-known worm strategy [29]—this is the update used here. After equilibration, we typically use 10^5 to 10^6 measurements on configurations separated by $\mathcal{O}(20)$ sweeps. The statistical errors we show are determined with the jackknife method, taking autocorrelation times into account.

For a first test we computed the energy density at vanishing chemical potential; cf. Eq. (16). In Fig. 1 we show the results for e at $\mu = 0$ as a function of the coupling J and compare to the weak and strong coupling expansions from Eq. (11). We find excellent agreement in the corresponding domains of J. This demonstrates that the mapping to the dual variables and the implementation of the dual Monte Carlo simulation are correct.

Likewise, the lattice mass gap am (at $\mu = 0$) has been determined in the usual manner from the decay of timelike correlators and was found to agree well with the critical chemical potential (see below).

We now switch to the situation where the dual approach is really essential, i.e., the simulations at nonzero chemical potential. In the top panel of Fig. 2 we plot the particle

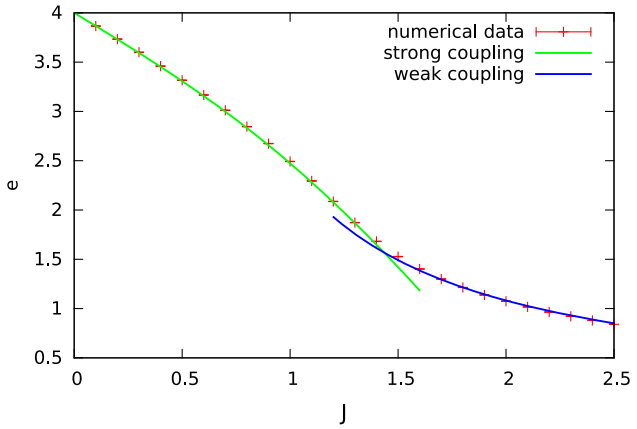

FIG. 1. Energy density versus the coupling at ($\mu = 0$). The analytical results for the strong and weak coupling expansions from Eq. (11) agree very well with the numerical results (having very small error bars) obtained from simulating the dual ensemble on a (10×10) lattice and using Eq. (16).

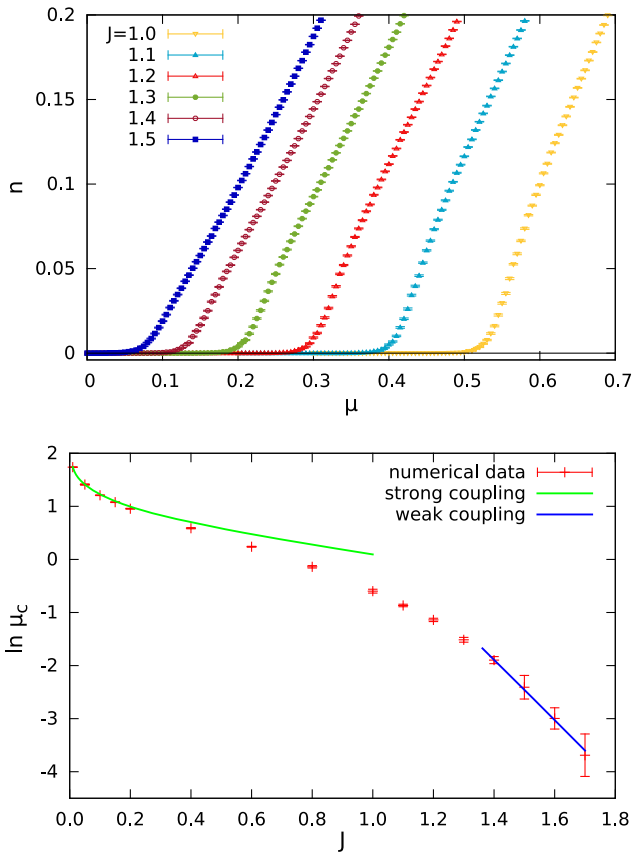

FIG. 2. Top: Expectation value of the particle number density versus the chemical potential μ, both in lattice units, at different couplings J for lattice size 90×90. Bottom: Logarithm of the corresponding critical chemical potentials as a function of the coupling. We compare our data to the strong coupling result $\ln(3/J)$ and the weak coupling expansion of the mass gap and Eq. (8), having obtained $C = 102(2)$ from a fit of the $J \geq 1.4$ data.

TABLE I. Results for the critical chemical potential values in lattice units used for normalizing.

J	0.01	0.05	0.1	0.2	0.4	0.6	0.8
$a\mu_c$	5.69(3)	4.10(5)	3.35(2)	2.60(2)	1.80(2)	1.27(1)	0.87(2)
J	1.0	1.1	1.2	1.3	1.4	1.5	1.6
$a\mu_c$	0.55(2)	0.42(1)	0.32(1)	0.22(1)	0.15(1)	0.09(2)	0.05(1)

density n measured via Eq. (14) as a function of μ. As a general phenomenon at low temperatures a net density is induced into the system only after μ has reached a threshold, the mass of the lightest particle with charge coupling to μ. The critical values of μ visible in that plot thus depend on the coupling J just like the mass. This is shown in the bottom panel of Fig. 2, again with strong and weak coupling expansions. For comparison we list the corresponding data in Table I.

The strong coupling behavior, $\mu = \ln(3/J)$ for $J \to 0$, is worked out in the Appendix, whereas the weak coupling result follows from the two-loop mass gap formula, Eq. (8), in which we obtain the constant C related to the UV cutoff by a one-parameter fit. The agreement is again very good, which is seen also in a comparison to the literature (Fig. 10 of [27]). Note also that the continuum scaling sets in at $J \simeq 1.4$, as for the energy density in Fig. 1: in particular from $J \sim 1.4$ on, the results for the energy density (Fig. 1) and the mass gap (Fig. 2) agree very well with the corresponding strong coupling curves (blue) that are valid in the continuum limit.

Most of our lattice data were taken at $J = 1.3$, where $am \sim 0.22$. This means a restriction to $\mu \ll 5m$; otherwise $a\mu$ becomes comparable to 1 and strong discretization effects set in.

B. Finite lattice phase diagram

Before we come to discussing continuum results, we first consider nonzero lattice spacing and finite volume; i.e., we study the system at fixed lattice size without a final continuum limit $J \to \infty$. We determine the J–μ phase diagram at low temperature, using the onset of nonzero particle density as a function of μ for determining the phase boundaries. Figure 3 shows this phase diagram for several critical chemical potentials. Note that the number of temporal sites is fixed, so the temperature in mass units $T/m = 1/(N_t am)$ varies with the coupling according to the mass gap formula $am(J)$, e.g., Eq. (8).

In [1] we have shown that close to the continuum limit at small temperatures and volumes, the particles are induced into the system one by one, displaying integer plateaus in the particle number itself (not its density). These transitions show up for large J and some examples are plotted in Fig. 3. The locations of these critical μ's are governed by the particle interaction phase shifts and thus contain interesting physics, as explained in detail in [1].

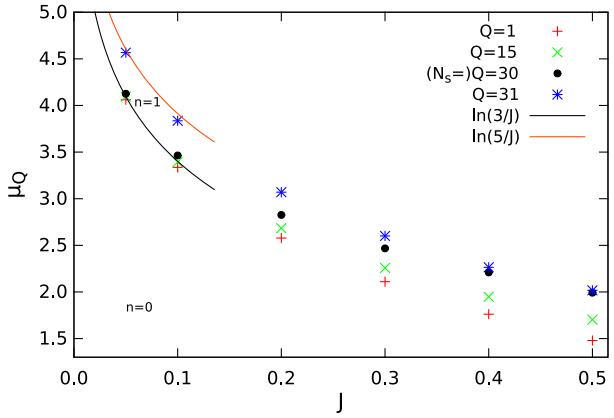

FIG. 3. Phase transition in the J–μ plane for $N_s = 30$ and $N_t = 1000$. At large J, i.e., towards the continuum limit, the critical chemical potentials with increasing index (from red to green to black to blue) induce individual transitions between integer charges as utilized in [1]. At small J the first N_s of them join to a single transition, $\mu_1 = \ldots = \mu_{Ns}$, increasing the particle *density* n in lattice units from 0 to 1 (see text). The next critical chemical potential μ_{N_s+1} (blue) is separated from those, and above it a density $n = 2$ will be induced. At large J, on the other hand, the change from μ_{Ns} to μ_{N_s+1} plays no particular role. The strong coupling predictions for the transitions $0 \to 1$ and $1 \to 2$ are included as solid curves.

In the strong coupling regime at small J the situation is different. In the dual representation of the partition function, Eq. (12), every dual variable is suppressed by the corresponding power of J. Still, the temporal components of the flux variable m are promoted by factors of e^{μ}, that eventually overcome the factors of $J/2$. This mechanism acts locally on every spatial site, which means that if it is preferable to have Q particles at some site ($m_{x,2} = Q$), then this immediately applies to all sites. In fact, the superposition of Q fluxes does not cost any action at strong coupling. Therefore, in this regime the particle number *density* changes by 1 (in lattice units). The corresponding critical values of μ depend on J logarithmically, and their values are computed in the Appendix. Figure 3 shows good agreement with these curves for small J and illustrates how intermediate couplings interpolate the transitions between these regimes. In particular all critical values of μ are on equal footing towards the continuum (large J), whereas in the strong coupling regime (small J) multiples of N_s bunch, such that regimes with fixed lattice density open up.

In Fig. 4 we show the lattice phase diagram with the quantity $J/2 \cdot \exp(\mu_Q)$ on the y-axis. In the strong coupling limit N_s critical μ's now meet at half integers $3/2$, $5/2$ etc., which agrees with the derivation in the Appendix again. The corresponding diagram for the O(2) model is shown in Fig. 3 of Ref. [12] (for this model the curves meet at integer values).

Let us conclude this subsection with a quick look at the third dual variable $k_{x,\nu}$, or more specifically at its sum K as

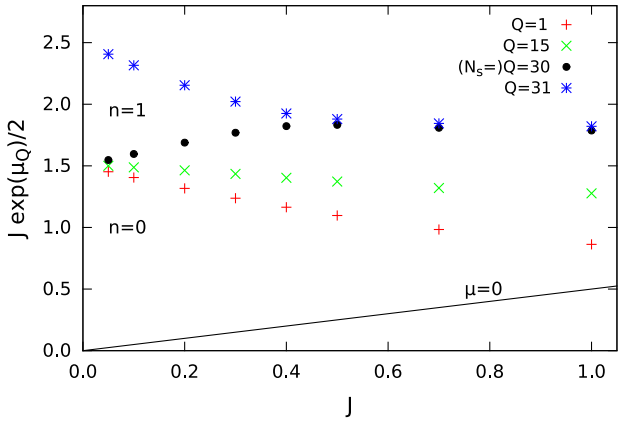

FIG. 4. Phase transition as in Fig. 3, but with a modified quantity on the y-axis (and some more data points for higher J's); see text.

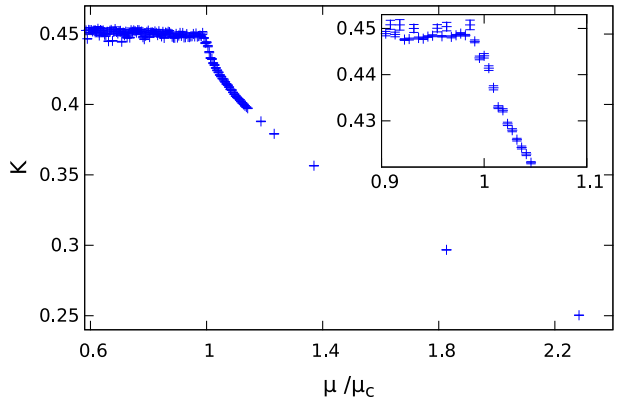

FIG. 5. Expectation value K for the third dual variable [for its definition and interpretation see Eq. (17) and below] also displaying a transition at $\mu = m$ ($J = 1.3$, $N_s = 200$, $N_t = 1000$). The value at small μ is the isotropic one related to the energy density by $K = J(4 - e)/6$.

defined in Eq. (17). For μ larger than the threshold the O(3) symmetry is explicitly broken to O(2) by the presence of the O(2) charge, which is expected to be manifest in a decrease of K [see the discussion below Eq. (17)]. In Fig. 5 we show K as a function of μ (normalized by μ_c) and indeed find the onset of a drop at the critical chemical potential, which confirms the picture that the system tends to become more and more planar as μ increases.

C. Crossover at nonzero temperature

We conclude the first analysis of the lattice model by studying the nature of the transitions mapped out in the previous subsection. For this study we still keep the temperature T fixed and perform the standard scaling analysis of order parameters with the spatial volume L to analyze the nature of the transition.

Figure 6 shows the particle number density (top panel) and its susceptibility (bottom panel) at a fixed low

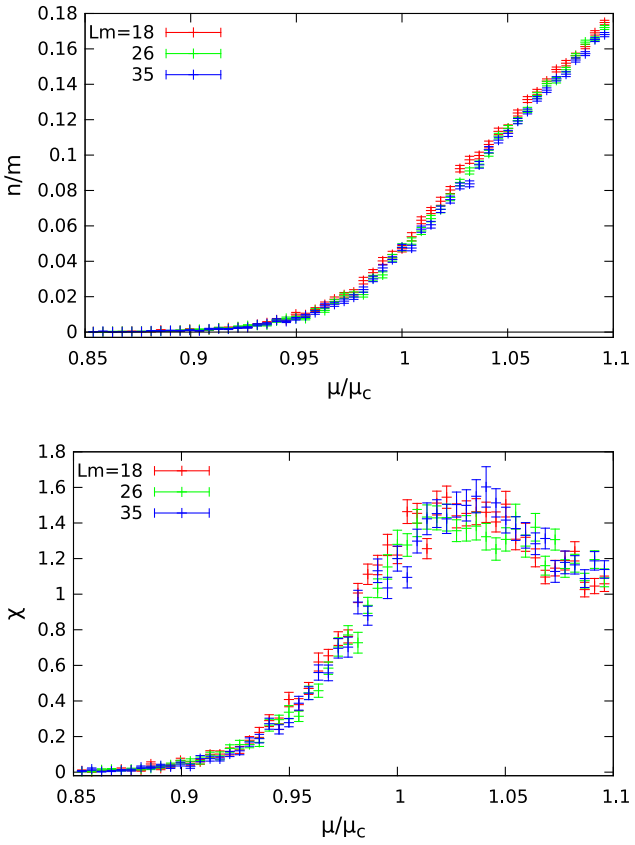

FIG. 6. Dependence of the particle number density and its susceptibility on the chemical potential at a fixed low temperature $T/m = 0.023$ for three spatial sizes' volumes (coupling $J = 1.3$, lattices with $N_t = 200$ and $N_s = 80$, 120, 160).

temperature of 2% of the mass. As a function of chemical potential μ the particle number n is monotonically increasing, with a strong variation emerging only above μ_c, while the susceptibility displays a maximum. Doubling the spatial size, the data still fall on top of each other for both observables. Equivalent results were found for two other nonzero temperatures, $T/m = 0.046$ and 0.011, and we conclude that for nonzero temperature the transition is smooth, i.e., it is a crossover.

IV. QUANTUM PHASE TRANSITION

We now explore the possibility of a quantum phase transition at zero temperature; i.e., we focus on the combined limit of zero temperature and infinite volume, i.e., $T = 0$, $L = \infty$, and analyze the transitions of the O(3) model as a function of the chemical potential. This amounts to sending the extents of both Euclidean time and space to infinity. Of course, with finite numerical simulations this can only be done as a limit, $T \to 0$ and $L^{-1} \to 0$. However, in general, the outcome depends on the particular choice of the trajectory towards that limit which one chooses in the T–L^{-1} plane. In particular the spatial and temporal correlation lengths can be different, as expressed by the

dynamical critical exponent (see Sec. IV B below). Thus we will discuss the behavior of the system for different "scaling trajectories," i.e., different paths leading to the limit $T = 0$, $L^{-1} = 0$. For these scaling trajectories we will present and interpret our data for the particle density and the spin stiffness. For the interpretation we will partly rely on simple model systems showing characteristic features observed in our simulations.

A. Scaling trajectories towards zero temperature and infinite volume and particle number results

As already outlined, when considering the limits $T \to 0$ and $L^{-1} \to 0$, the behavior of the system will depend on the particular scaling trajectory one follows in the T–L^{-1} plane towards the origin. These limits can be taken in different ways, and a possible choice is to take the $L^{-1} \to 0$ limit first, keeping temperature fixed, and then take $T \to 0$. We can also keep L fixed and take $T \to 0$ first, and then $L^{-1} \to 0$. More generally we can take the limit T, $L^{-1} \to 0$, keeping

$$TL^{\alpha} = \text{const.} \tag{19}$$

fixed, where α is a non-negative real number. Generically, the constant has a noninteger mass dimension; for the practical implementation (e.g., for $\alpha = 2$ below) one can fix $(T/m)(Lm)^{\alpha}$ to a dimensionless constant. Notice that the consecutive limits mentioned above correspond to the limiting cases $\alpha = 0$ and $\alpha = \infty$. Here we will consider these two scaling trajectories plus $\alpha = 1, 2$ as we illustrate in Fig. 7. In this subsection we briefly discuss these different scaling trajectories and partly describe the resulting physics using model calculations for the behavior at the emerging phase transitions.

In the limiting trajectories $\alpha = 0$ and $\alpha = \infty$ one has to perform the two limits consecutively. This is difficult to implement on the lattice but reveals interesting physics. Therefore, we will use simple model calculations to illustrate characteristic features of the consecutive limits. We will compare our numerical data to results for *free one-dimensional fermions*: At low densities the behavior is governed by the small momentum exchange between the particles, which for the O(3) model at hand are one-dimensional repulsive bosons. At low momentum their behavior is universal and given by free (spinless) fermions; see Sec. V.

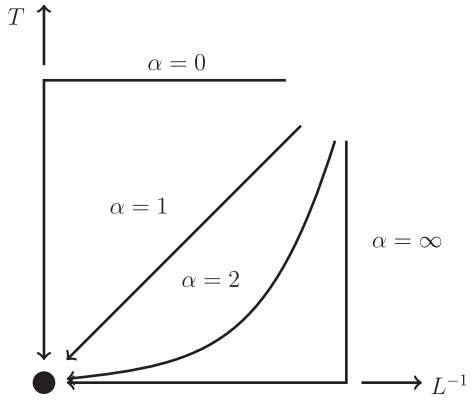

FIG. 7. Illustration of the four scaling trajectories in the T–L^{-1} plane towards the zero temperature and infinite volume limit (black dot) which we use in this study [see discussion around (19)].

For the other two scaling trajectories, $\alpha = 1$ and $\alpha = 2$, the results will not differ much concerning the particle density, but are characterized by a different behavior of the spin stiffness, which we will discuss in detail in Sec. IV B.

The scaling trajectory $\alpha = 0$: The $\alpha = 0$ trajectory corresponds to the consecutive limits

$$L^{-1} \to 0 \text{ at fixed } T, \quad \text{then } T \to 0.$$

The first limit of this sequence corresponds to the finite volume scaling at fixed nonzero temperature studied in Sec. III C. This analysis has revealed a crossover as seen from Fig. 6. Actually every fixed temperature possesses a specific crossover curve $n(\mu)_T$, which upon lowering the temperature T to zero in the second limit might become steeper near some μ_c and turn into a genuine phase transition. To some extent this feature is seen in our data shown in Fig. 9 below, where it is, however, overlaid by the formation of "condensation steps" (see the discussion below).

The emergence of such a quantum phase transition as T approaches 0 is of course a well-known feature which already appears in the simple model of free fermions in one spatial dimension: the density n is given by the Fermi-Dirac integral ($L^{-1} = 0$),

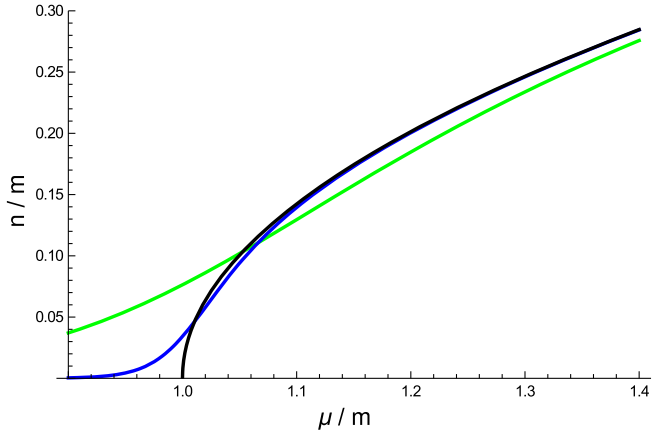

FIG. 8. Emergence of a phase transition in the limit $T \to 0$ for free one-dimensional fermions in an infinite volume. We show that the smooth curves for $T/m = 1/10$ (green) and $T/m = 1/50$ (blue) approach the $T = 0$ square-root behavior from Eq. (21). This is a model calculation for the scaling trajectory $\alpha = 0$, especially its second limit $T \to 0$ at $L^{-1} = 0$.

$$n_f = \int_{-\infty}^{\infty} \frac{dk}{2\pi} \frac{1}{1+\exp((m+k^2/2m-\mu)/T)}, \tag{20}$$

where we use a nonrelativistic dispersion which is sufficient for a first illustration. The density can be expressed by a polylogarithm $\mathrm{Li}_{1/2}$, from which one obtains a square root in the $T \to 0$ limit,

$$\frac{n_f}{m} \to \frac{\sqrt{2}}{\pi}\sqrt{\mu/m-1}\cdot\Theta_{\mathrm{Heaviside}}(\mu/m-1) \quad \text{for } L^{-1}=0, T\to 0. \tag{21}$$

The square-root behavior, which is nonanalytic at $\mu/m=1$, is indeed reached only for $T=0$ via a sequence of analytic crossover-type curves as shown in Fig. 8.

The scaling trajectory $\alpha=\infty$: We have already pointed out that our results for the density as a function of μ start to show "condensation steps" when the temperature T is lowered at fixed L. Thus it is interesting to study also the scaling trajectory $\alpha=\infty$, which is defined by the consecutive limits

$$T\to 0 \text{ at fixed } L, \quad \text{then } L^{-1}\to 0.$$

Our numerical results for the first of these two limits are shown in Fig. 9. When lowering the temperature T at fixed L we observe the emergence of plateaus in the density where the particle numbers are integers. The plateaus correspond to sectors with fixed particle number, and are smoothed out by the finite temperature (the width of the transition region being proportional to the temperature). Therefore, sharp *steps* emerge in the $T\to 0$ limit at any fixed L.

After considering $T=0$ at finite L, i.e., following the $\alpha=\infty$ trajectory, we need to perform the second limit $L^{-1}\to 0$. Also the behavior of this second limit can be illustrated in a one-dimensional fermion model, the Tonks-Girardeau limit of the Lieb-Liniger system, which we discuss in detail in Sec. V. One finds that the minimal energy in each particle number sector Q is $E^{(Q)}_{\mathrm{min}} = \pi^2/(6L^2m)\cdot(Q^2-1)Q$. Steps occur whenever $E^{(Q)}_{\mathrm{min}} - Q\mu = E^{(Q-1)}_{\mathrm{min}} - (Q-1)\mu$ and thus are located at $\mu_Q = m + \pi^2/2\cdot Q(Q-1)/(L^2m)$. The corresponding density $n/m = 1/Lm\cdot\sum_{Q=1}^{\infty}\Theta_{\mathrm{Heaviside}}(\mu-\mu_Q)$ is shown in the top panel of Fig. 10. It "oscillates" around its square-root limit, reaching it by ever smaller oscillations. The square root can also be seen analytically, since for large Q the steps are at $\mu_Q/m = 1+\pi^2/2\cdot(n/m)^2$.

The same behavior is seen in our numerical O(3) data shown in the bottom panel of Fig. 10, where, in the same fashion, "oscillations" around a limiting curve diminish with increasing L. However, this can only be done at low but nonzero temperatures and, as discussed above, this gives rise to a crossover instead of a phase transition.

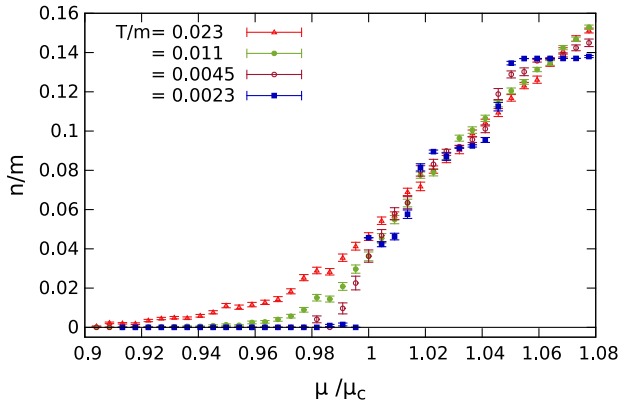

FIG. 9. Particle density n in units of the mass as a function of μ for different temperatures at a fixed volume of $L=22/m$ ($J=1.3$, $N_s=100$, $N_t=200$, 400, 1000, 2000). When lowering the temperature one observes [1] the emergence of plateaus at integer values of the particle number, which for the normalized density n/m used here corresponds to integer multiples of 0.046.

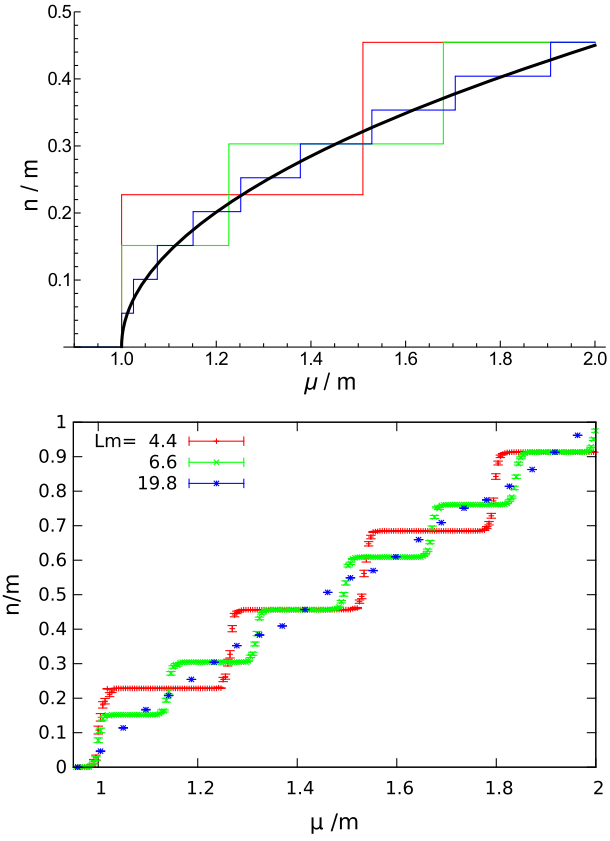

FIG. 10. Illustration of how the low temperature density with its steps at any finite volume approaches its infinite volume limit. Top: The Tonks-Girardeau gas similar to free fermions at zero temperature (see text) for $Lm=4.4$, 6.6, 19.8 (red, green, blue) being a model calculation for the scaling trajectory $\alpha=\infty$ (second limit). Bottom: Our results for the O(3) model at $T/m=0.0023$. For the different scales recall that free fermions approximate the O(3) model only at low densities.

TABLE II. Lattice extensions, temperature and spatial extent for the two scaling trajectories $\alpha = 1$ and $\alpha = 2$ (at $J = 1.3$ for which $am = 0.22$).

Scaling trajectory	N_t	N_s	T/m	Lm
$\alpha = 1$	80	80	0.057	18
$[T = L^{-1}]$	160	160	0.029	35
	320	320	0.014	70
$\alpha = 2$	400	40	0.011	9
$[T/m = 0.88/(Lm)^2]$	1600	80	0.0028	18
$[Lm = 0.94/\sqrt{T/m}]$	6400	160	0.0007	36

The scaling trajectories $\alpha = 1$ and $\alpha = 2$: In the scaling trajectories $\alpha = 1$ and $\alpha = 2$ we consider approaches to the limit $T = 0$, $L^{-1} = 0$ by sending T and L^{-1} to zero simultaneously. The trajectories differ in their functional relation between T and L:

$$\alpha = 1\colon\ T \to 0 \quad \text{and} \quad L^{-1} \to 0 \quad \text{with} \quad T = L^{-1}$$
$$\alpha = 2\colon\ T \to 0 \quad \text{and} \quad L^{-1} \to 0 \quad \text{with} \quad T \propto (L^{-1})^2.$$

Obviously $\alpha = 1$ corresponds to square lattices $N_t = N_s$, while $\alpha = 2$ corresponds to time elongated lattices with $N_t \propto (N_s)^2$. To be specific, in our numerical simulations for $\alpha = 2$ we have used $N_t = (N_s/2)^2$ at $J = 1.3$ ($am \sim 0.22$), which amounts to $T/m = 0.88/(Lm)^2$ or $Lm = 0.94/\sqrt{T/m}$. We summarize the parameters of the simulations used for the analysis of the $\alpha = 1$ and $\alpha = 2$ trajectories in Table II.

Figure 11 shows our simulation results for these two scaling trajectories. We show the particle density n as a function of μ for $T \to 0$ and $L \to \infty$ simultaneously. One can see in both trajectories that n vanishes for values of μ smaller than the threshold m, while it approaches certain nonzero values for $\mu > m$. This is an indication for a nonanalyticity developing at $\mu = m$ in the limit $T \to 0$, and thus for a quantum phase transition. Whether it emerges in the form of a jump in n (first order transition) or an infinite slope (second order) cannot be decided with our current data (and the common infinite volume limit $L \to \infty$ to distinguish the orders is part of the scaling to zero temperature). The agreement with analytic predictions for repulsive bosons presented in Sec. V indicates a square-root dependence on μ and thus a second order transition.

Moreover, the data at lowest T/highest L do not differ much between $\alpha = 1$ and $\alpha = 2$. This bulk quantity therefore does not seem too sensitive to the particular scaling trajectory in the limit $T \to 0$ and $L \to \infty$.

B. Spin stiffness and dynamical critical exponent

Figure 12 shows our spin stiffness data for the two scaling trajectories $\alpha = 1$ and $\alpha = 2$. Qualitatively, the stiffness behaves like the density: it vanishes for $\mu < m$ and is nonzero for $\mu > m$. In contrast to the density, however,

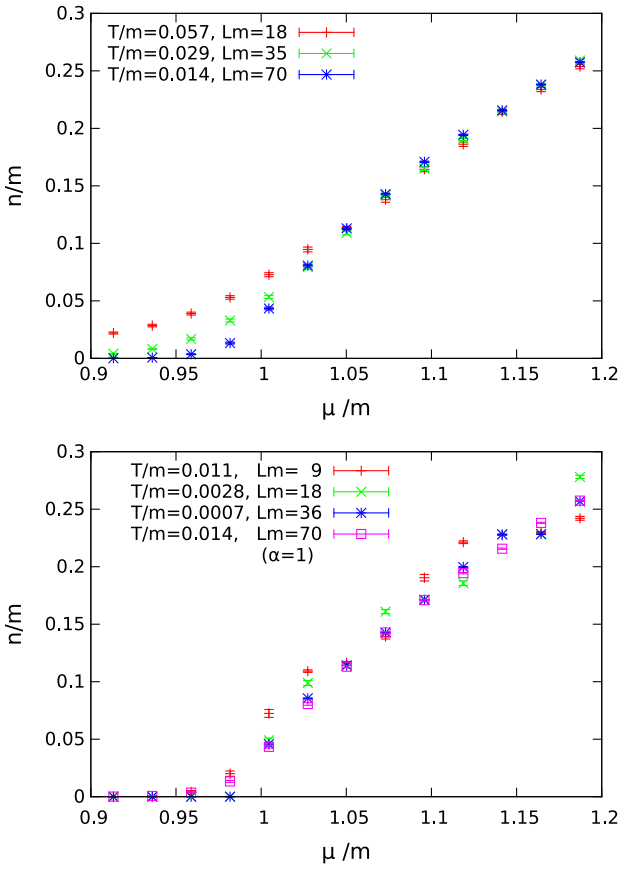

FIG. 11. Particle number density for the $\alpha = 1$ (top) and $\alpha = 2$ (bottom) scaling trajectories, both at $J = 1.3$. For $\alpha = 1$ we approach $T = 0$ using $L = 1/T$, whereas for $\alpha = 2$ $L \sim T^{-1/2}$ increases less rapidly. In the $\alpha = 2$ panel we also include the lowest T data from $\alpha = 1$ for comparison. For the lattice parameters see Table II.

the stiffness shows a clear dependence on α: for $\alpha = 1$ it is *significantly smaller* in the $\mu > m$ phase than for $\alpha = 2$. In addition, the stiffness *agrees* with the density (divided by mass) for $\alpha = 2$ at small densities, as Fig. 13 shows. Our stiffness data do not display the signature of a BKT transition for $\mu > m$ in the spatial correlations suggested in [7].

Let us now come to the interpretation of these data. It is known that the stiffness depends on the order of the limits $T \to 0$ and $L \to \infty$ [30]: when $L \to \infty$ is taken first (i.e. $\alpha = 0$ scaling) the stiffness vanishes, whereas when $T \to 0$ is taken first (i.e. $\alpha = \infty$ scaling) it approaches the susceptibility of the ground state with respect to the same twist.

For $\alpha = 0$ one keeps the temperature fixed (and thus the transition is a crossover), and then increases the spatial size to infinity. It is clear that in this way one loses all spatial correlations, the twist at the spatial boundary has no effect on the free energy for $L \to \infty$ and the stiffness vanishes (the successive limit of zero temperature cannot change this any more). Our data for $\alpha = 1$ suggest that this scaling trajectory is similar to $\alpha = 0$ since the system size is

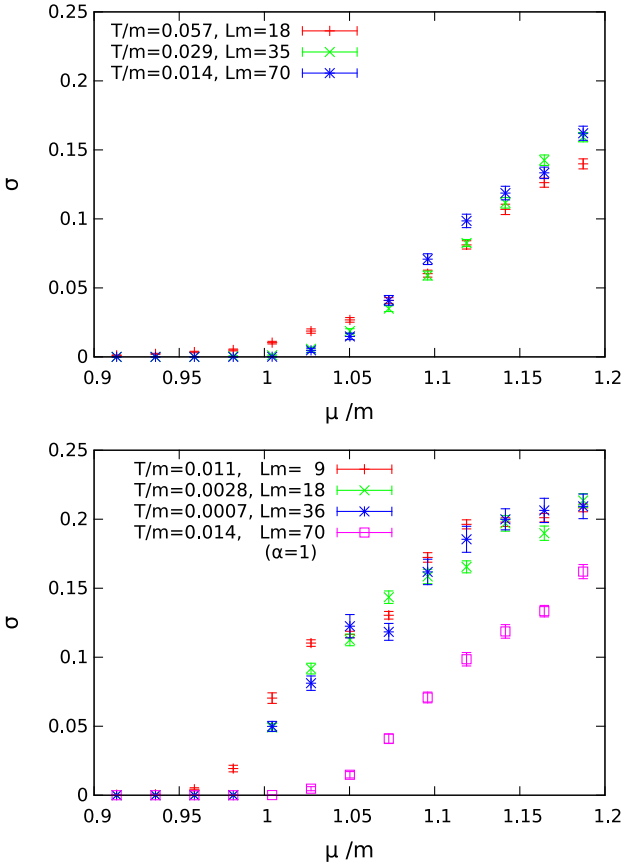

FIG. 12. Spin stiffness for the $\alpha = 1$ (top) and $\alpha = 2$ (bottom) scaling trajectories. As in Fig. 11 we include the lowest T data from $\alpha = 1$ in the $\alpha = 2$ panel. For the lattice parameters see Table II.

growing too fast in comparison to $T \to 0$, such that spatial correlations are lost, leading to a small stiffness.

For $\alpha = \infty$ one considers the zero temperature system at fixed volume and only afterwards the size is increased. At zero temperature one expects the ground state to determine the thermodynamic properties. In fact, the system at finite L is gapped proportional to $1/L^2$. Therefore, the partition function in the $T \to 0$ limit is dominated by the ground state, and the free energy becomes the ground state energy (noting that the latter is T-independent; this is nothing but the third law of thermodynamics). As a consequence, the stiffness is the susceptibility of the ground state with respect to the spatial twist, as mentioned above.

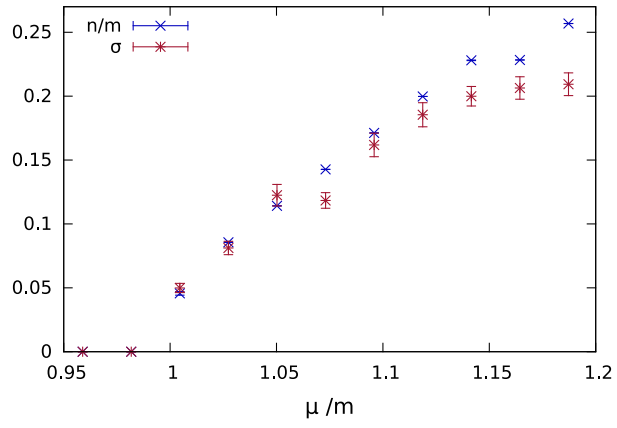

FIG. 13. Agreement of stiffness and density (in mass units) close to zero temperature in a large volume $L \sim 1/\sqrt{T}$ ($\alpha = 2$, time elongated lattice): $T/m = 0.0007$, $Lm = 36$.

On top of that, we now invoke an argument from the Bethe *Ansätze* of Sec. V. One can easily convince oneself[3] that the (nonrelativistic) pseudomomenta k_i in the presence of a spatial twist φ are shifted by φ/L. The ground state energy $\sum_{i=1}^{Q} k_i^2/(2m)$ receives no linear term in φ since the total momentum $\sum k_i$ vanishes. The quadratic term is the constant $Q \cdot (\varphi/L)^2/(2m)$, and we immediately obtain the stiffness as $\sigma = Q/(Lm) = n/m$. This explains that the *stiffness equals the density* for $\alpha = \infty$, for small densities. Our data for $\alpha = 2$ suggest that this scaling trajectory is similar to $\alpha = \infty$ since the stiffness still equals the density, as seen in Fig. 13.

Finally, let us discuss the *dynamical critical exponent* [31] z that results from our findings. The correlation length near a second order phase transition is known to diverge. To achieve $T = 0$ in the study of the quantum phase transition one has to send the extent N_t of the Euclidean time to infinity. We remark that for the discussion of the continuum scaling formulas below we use the continuum notation with $\beta = 1/T$ for the inverse temperature and identify (in lattice units) $\beta \equiv N_t$. Only at $N_t = \beta = \infty$ does the phase transition occur and the spatial correlation length ξ is infinite. However, the system also has a typical correlation length ξ_τ in the Euclidean time direction. If nothing in the system distinguishes between space and Euclidean time, the two correlation lengths have to agree (which corresponds to $z = 1$ below). However, in general—and in particular in the presence of μ which breaks the Euclidean symmetry by coupling to temporal components/winding numbers—the two correlation lengths are related by $\xi_\tau \sim \xi^z$ with z the dynamical critical exponent [31]. Note the similarity to our scaling trajectories $\beta \sim L^\alpha$ and indeed our stiffness data can be used to determine z and the correlation length critical exponent ν. For that we use finite size scaling of the free energy density [32],

$$f \sim \frac{1}{L\beta} g\left(\frac{\xi}{L}, \frac{\xi^z}{\beta}; \varphi\right), \tag{22}$$

[3]The I_i in Eq. (26) comes from closing the boundary and thus need to be shifted by $\varphi/(2\pi L)$. Moreover, it is sufficient to consider the nonrelativistic Bethe *Ansatz* and thus replace $\theta \approx k/m \approx \sinh(\theta)$. Then the I_i-shift can be transferred to a uniform shift in the k_i, because the Δ-term contains differences of k's only and thus is unchanged.

where the prefactor is the inverse volume (in $1+1$ dimensions), making $f = F/L$ an intensive quantity, and g is a universal function of the spatial correlation length, the box sizes and the twist angle. Again, non-integer dimensions can be compensated by the corresponding powers of the mass. Using the scaling $\xi \sim \delta^{-\nu}$ with the normalized distance to the critical value $\delta = \mu/m - 1$ and the definition (6), we get for the stiffness

$$\sigma \sim L^{1-z} h(L^{1/\nu}\delta, TL^z) \tag{23}$$

where h is another universal function.

For practical purposes one can derive two criteria [33]:

(a) the curves μ vs $L^{z-1}\sigma$ intersect at $\mu = m$, if TL^z is kept constant,

simply because at $\delta = 0$ the length L does not enter as the argument of h anymore and

(b) the curves $L^{1/\nu}\delta$ vs $L^{z-1}\sigma$ collapse to a single curve, again if TL^z is kept constant.

Our data are collected at constant TL^α with $\alpha = 1, 2$ and thus we can ask whether $z = 1$ or $z = 2$ obeys these statements, at least approximately. We will rescale all dimensionful quantities by the corresponding power of mass.

For statement (a) with $z = 1$ we thus plot $\sigma(\mu)$, keeping TL constant, i.e., on the scaling trajectory $\alpha = 1$, while for $z = 2$ we plot $L^1\sigma(\mu)$, keeping TL^2 constant, i.e., on the scaling trajectory $\alpha = 2$, and see whether the data for different L's intersect. As Fig. 14 shows, the data certainly do not intersect for $z = 1$. For $z = 2$ the curves intersect pairwise (albeit at a value of μ slightly smaller than m) when naively interpolated linearly. To completely resolve this regime, more accurate data (at more chemical potential values and in the continuum limit) and a better interpolation are needed. Note the inverted order of the data points when crossing the critical chemical potential, which is the reason for the intersections we see and which is absent for $z = 1$. We expect that this feature will remain also for more accurate data and that, therefore, an exponent $z = 2$ describes the scaling better than $z = 1$.

For statement (b) one has to deal with the appearance of another critical exponent ν. In Fig. 15 we plot the observables of this statement assuming the value $\nu = 1/2$ for free fermions. Again a collapse to a single curve describes the situation much better for $z = 2$. This is consistent with the finding that σ equal to n/m (for the $\alpha = 2$ data, see Fig. 13) follows the square-root behavior of Eq. (21) (see also Sec. V below). As a consequence of the square-root behavior, the $\alpha = 2$ data collapse for any (z, ν)

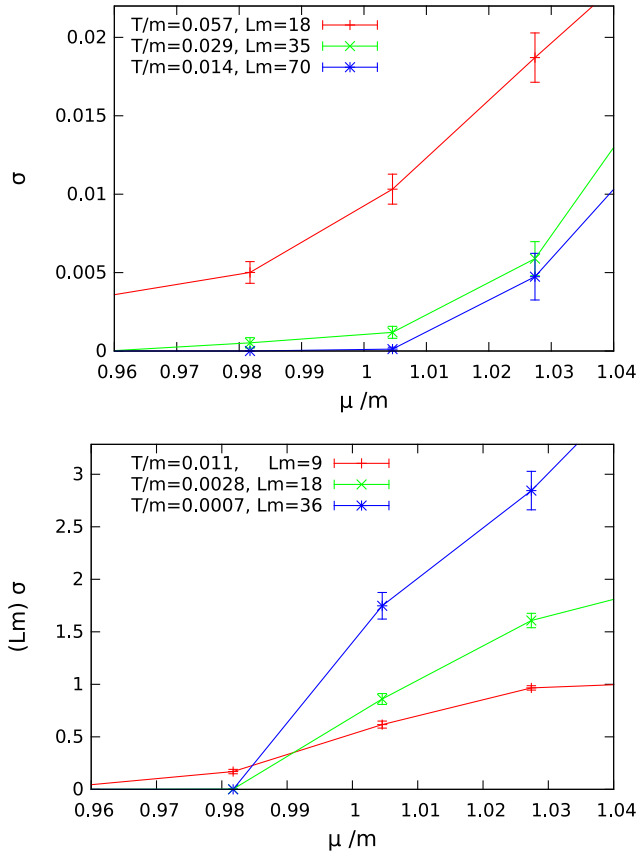

FIG. 14. Numerical checks of statement (a) for exponents $z = 1$ (top) and $z = 2$ (bottom). For the lattice parameters see Table II.

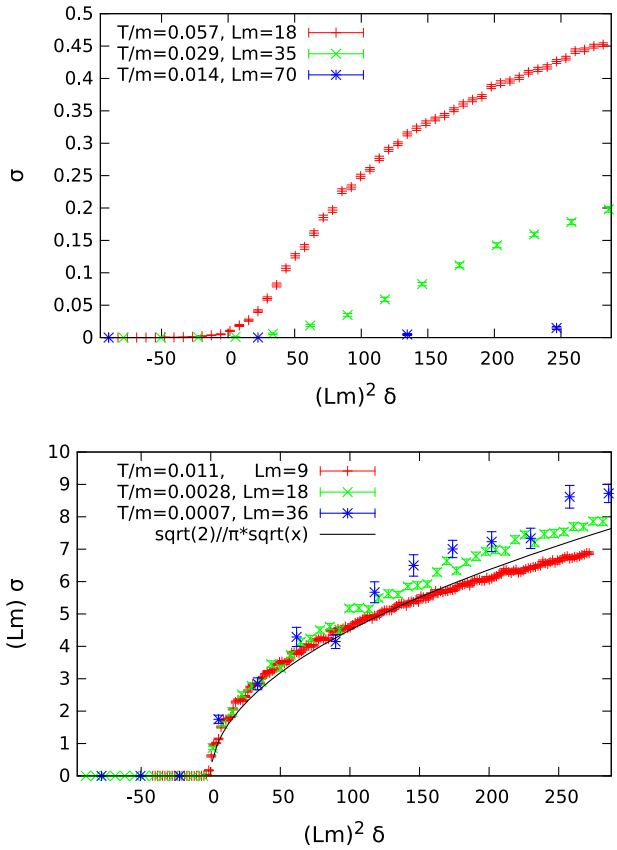

FIG. 15. Numerical checks of statement (b) for $z = 1$ (top) and $z = 2$ (bottom) assuming $\nu = 1/2$. In the bottom panel we also include the square-root behavior in these variables. For the lattice parameters see Table II.

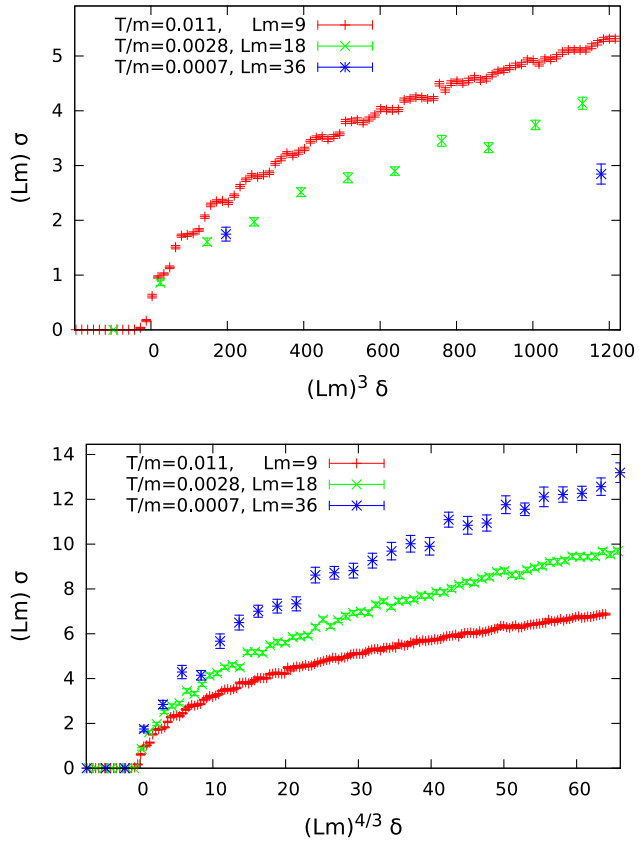

FIG. 16. Numerical checks of statement (b) assuming $z = 2$ for $\nu = 1/3$ (top) and $\nu = 3/4$ (bottom). For the lattice parameters see Table II.

with $1/\nu = 2(z-1)$. Finally, we can assume $z = 2$ and check the value of ν away from $1/2$. Figure 16 shows data proposing $\nu = 1/3$ and $\nu = 3/4$, for which the curves certainly do not collapse.

From this analysis we conclude that the critical exponents of the O(3) quantum phase transition at $\mu = m$ are consistent with $z = 2$ and $\nu = 1/2$, the values of free 1d fermions.

V. COMPARISON TO ANALYTIC RESULTS ON REPULSIVE BOSONS

In this section we will compare our density data to the density for systems of repulsive bosons in one spatial dimension. One of the best-known examples is the one introduced by Lieb and Liniger (LL), where boson pairs interact via a Dirac delta function [13]. The system can be solved in terms of plane waves picking up phase shifts δ when two bosons are interchanged. Such a Bethe *Ansatz* [34] works for nonrelativistic or relativistic bosons, without antibosons though.

The phase shifts of the O(3) model are also known [35] and those of "isospin 2,"

$$\delta = -\arctan\frac{\pi}{2\theta}, \tag{24}$$

with the relative rapidity,

$$\theta = \operatorname{arsinh}(k/m), \tag{25}$$

govern the low density regime [1,22]. We will thus use the Bethe *Ansatz* equations with those phase shifts. Note that the O(3) wave functions are not plane waves anymore, but the Bethe *Ansatz* is believed to give an exact result at low densities [36].

At very low momenta the O(3) phase shifts agree with those of the LL model; actually all repulsive one-dimensional bosons are universal in the deep IR, where the precise UV shape of the interaction is not relevant and where $\delta(0) = -\pi/2$ by Levinson's theorem [37]. Using only this value one arrives at the Tonks-Girardeau (TG) gas, which is the infinite coupling limit of the LL model [14,15]. Its eigenvalues are known to be those of free fermions with the modification that the numbers I_i in Eq. (26) below are not always half-integers as is the case for antiperiodic fermions (which is not relevant for large L) and that the eigenfunctions of the TG gas are still symmetric under the exchange of bosons. We have already shown that this results in the square-root behavior (21) of the particle density for $\mu \approx m$ at zero temperature and infinite volume [see also Eq. (31) below].

To be more precise, the relativistic Bethe *Ansatz* reads

$$Lm\sinh(\theta_i) - 2\sum_{\substack{j=1\\ j\neq i}}^{Q}\Delta(\theta_j - \theta_i) = 2\pi I_i, \tag{26}$$

where the I_i are distinct, and half-integer/integer for even/odd total charge Q. In our conventions the dynamics enters via the phase shifts in

$$\Delta = \delta + \pi/2 \tag{27}$$

with $\lim_{k\to 0}\Delta = 0$. This *Ansatz* works for ground states [with the choice $\{I_i\} = \{-(Q-1)/2, \ldots, (Q-1)/2\}$] and excited states at fixed particle number Q in any finite volume L. The nonrelativistic Bethe *Ansatz* can be obtained by approximating the rapidities as $\theta \approx k/m$. Both are not too hard to solve numerically.

Furthermore, Yang and Yang have derived a thermodynamic Bethe *Ansatz* for the density $\rho(k)$ and energy density $\epsilon(k)$ at nonzero temperatures and chemical potentials [16] in infinite volumes. The nonrelativistic Yang-Yang equations give rise to

$$2\pi\rho(k)[1 + e^{\epsilon(k)/T}] = 1 + \int_{-\infty}^{\infty} d\tilde{k}\rho(\tilde{k})\Delta'(k-\tilde{k}), \tag{28a}$$

$$\epsilon(k) = \frac{k^2}{2m} + (m-\mu) - \frac{T}{\pi}\int_{-\infty}^{\infty} d\tilde{k}\log(1 + e^{-\epsilon(k)/T})\Delta'(k-\tilde{k}), \tag{28b}$$

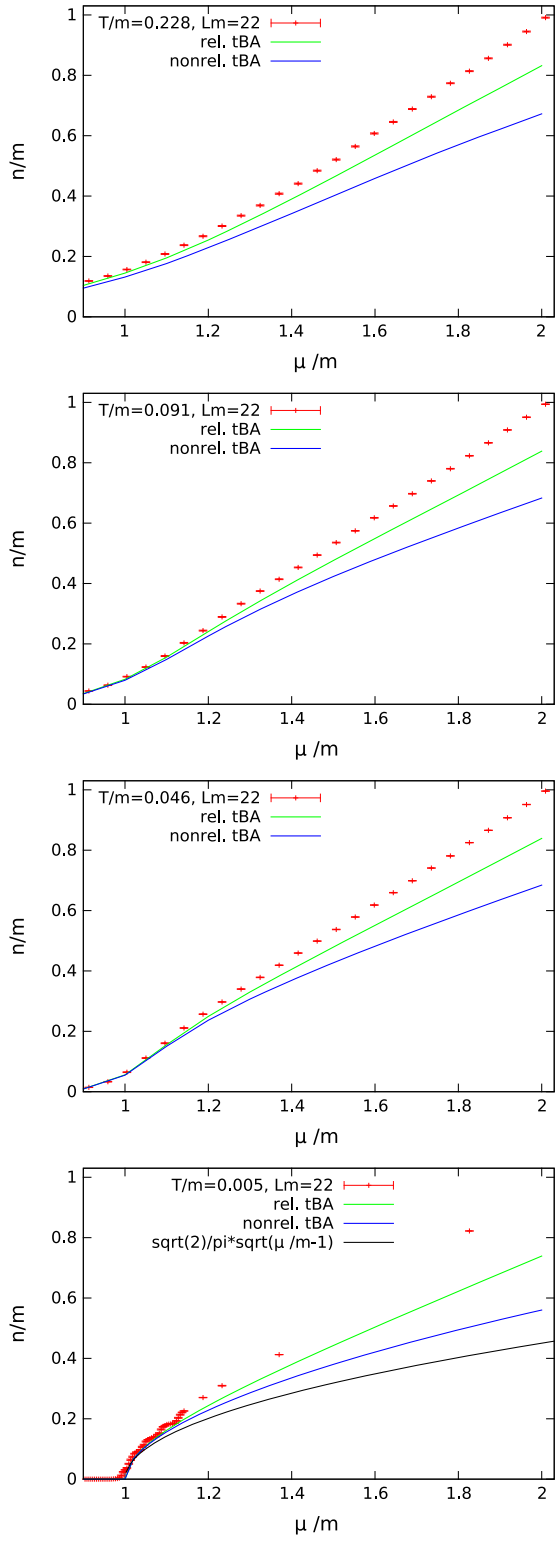

FIG. 17. The density n/m vs chemical potential μ/m at temperatures $T/m = 0.228,\ 0.091,\ 0.046,\ 0.005$ from top to bottom. We compare the numerical evaluation of the relativistic Bethe *Ansatz* equation (29) (green curve) and the nonrelativistic Bethe *Ansatz* equation of (28) (blue curve), with the lattice data (red symbols, $J = 1.3$, $N_s = 100$ and $N_t = 20,\ 50,\ 100,\ 1000$). The black line in the bottom plot is the universal square-root behavior given in (31).

while, following similar arguments of [16], and ignoring thermal pair production,[4] the relativistic Yang-Yang equations read

$$2\pi\rho(\theta)(1+e^{\epsilon(\theta)/T}) = m\cosh\theta + 2\int_{-\Theta}^{\Theta} d\tilde{\theta}\rho(\theta)\Delta'(\theta-\tilde{\theta}), \tag{29a}$$

$$\epsilon(\theta) = m\cosh\theta - \mu - \frac{T}{\pi}\int_{-\Theta}^{\Theta} d\tilde{\theta}\log(1+e^{-\epsilon/T})\Delta'(\tilde{\theta}). \tag{29b}$$

In both relativistic and nonrelativistic equations, $\Delta'(x) = \frac{d\Delta(x)}{dx}$, where Δ is defined by (27). Having solved this system one can extract the particle density as $n = \int_{-\infty}^{\infty} d\tilde{k}\rho(\tilde{k})$.

Finally, the zero temperature limit for the density is

$$2\pi\rho(k) = 1 + \int_{-K}^{K} d\tilde{k}\rho(\tilde{k})\Delta'(k-\tilde{k}),$$
$$\rho(|k| > K) = 0, \tag{30}$$

where K is the analogue of the Fermi momentum related to μ by $K = \sqrt{2}m\sqrt{\mu/m-1}$. Low densities amount to $\mu \approx m$ and thus $K \to 0$, for which the integration range shrinks, $\rho(0) = 1/(2\pi)$ and $n = \rho(0)2K$, such that

$$\frac{n}{m} = \frac{\sqrt{2}}{\pi}\sqrt{\mu/m-1} \quad (T=0, \text{small } n/m), \tag{31}$$

confirming once more the square-root behavior for low densities.

We solve these integral equations numerically and compare to the lattice data in Fig. 17. The agreement is fairly good. Note that these are parameter-free *Ansätze*, so no fit is involved in the comparison. Let us repeat that the agreement is expected for low temperatures only, since Bethe *Ansätze* do not contain antibosons and pair production.

VI. SUMMARY

In this paper we have presented thermodynamic lattice simulations of the asymptotically free two-dimensional O(3) model. The complex action problem of the conventional representation at finite chemical potential is overcome by using a representation in terms of dual variables; i.e., we simulated worldlines. In the O(3) model the mass of the particle triplet is generated dynamically, and in our simulations we have confirmed the expectation that at low

[4]Because of this, the equations are only exact at zero temperature. Nevertheless we will use them at finite, but small temperature to compare to lattice data.

temperatures a nonzero particle number (or charge) density occurs only when μ reaches the threshold given by the mass. Furthermore, in small volumes several critical values of μ occur which correspond to integer particle numbers induced by μ [1] (for finite lattice couplings see the lattice phase diagram in Sec. III B).

A finite volume scaling analysis has revealed that at nonzero temperatures the particle density as a function of μ is regular; i.e., the transition is a crossover. The possibility of a phase transition at zero temperature has been analyzed through a simultaneous scaling of Euclidean time and space. Indeed, the data indicate a quantum phase transition at $\mu = m$, which, using the agreement with Bethe *Ansätze* for one-dimensional repulsive bosons, should be of second order because the particle density follows the universal square-root behavior. Further comparisons to these *Ansätze* have shown that the O(3) model can indeed be described by these bosons, including the crossover behavior at nonzero temperature.

We stress that for a more complete analysis of the physical picture presented here a systematic continuum limit has to be performed by increasing J and the lattice volume accordingly. So far this has been done only in some exploratory runs and the results confirm the physical picture presented here, although a systematic continuum limit has to be postponed to future work. Also the fact that in [1] it was found that the $J = 1.3$, 1.4 and 1.5 results agree supports the claim that the physical picture presented here is already the continuum one.

We have also measured the spin stiffness which in the conventional representation is defined via twisted spatial boundary conditions and in the dual representation measures spatial winding numbers of the worldlines. Based on the boson description at zero temperatures with only ground states, the stiffness is expected to be equal to the particle density. This is consistent with our low temperature data, when scaling L such that TL^2 is constant, i.e., $\alpha = 2$. However, when L is larger in the zero temperature limit, e.g., when TL is kept constant, i.e., $\alpha = 1$, then this equality does not hold and the spin stiffness is significantly lower, which indicates a lost correlation between the spatial boundaries. From these findings we conclude that the dynamical critical exponent z is close to 2, in agreement with free fermions.

Although originally introduced for studying a potential BKT transition, our stiffness data have not indicated such a transition in the O(3) system at chemical potentials larger than the mass where it tends to be planar (as we have also confirmed). In [7] it was suggested that the O(3) model may enter an effective O(2) model in two phases: the vortex percolating or the vortex pairing regime, which are separated by a BKT-like transition affecting the mass of the underlying condensing particles. Unlike the case of the zero density O(2) model, the measurements of stiffness which we performed here cannot distinguish between these two phases, because as we saw in one-dimensional finite density systems the stiffness is very sensitive to the way zero temperature and infinite volumes are taken, and is not simply an indicator of the mass of the underlying particles (i.e., whether or not vortices percolate).

Besides higher precision, further studies in various directions would be useful: First of all, perturbation theory should match our lattice data at high μ's (keeping $a\mu$ small to avoid discretization effects). Secondly, measuring the vortex correlation functions or the topological susceptibility should shed light on the possibility of a BKT-like transition. Extensions to higher O(N) or CP(N-1) models as well as to $2+1$ dimensions could be done straightforwardly with the dual representation.

The physically very interesting regimes of complex chemical potentials, where fractional instantons should occur (which in turn underly the resurgence program mentioned in the Introduction), and at large theta angle, with the Haldane conjecture of a phase transition at theta angle equal to π, remain a challenge, as the dual variables used here do not solve the sign problem in these situations.

ACKNOWLEDGMENTS

We thank Quirin Hummel, Yannick Meurice, Lode Pollet, Klaus Richter, Juan Diego Urbina, Andreas Wipf and in particular Hans-Gerd Evertz for helpful discussions. F. B. is supported by the DFG (BR 2872/6-1) and T. K. by the Austrian Science Fund, FWF, DK *Hadrons in Vacuum, Nuclei, and Stars* (FWF DK W1203-N16). Furthermore this work was partly supported by the Austrian Science Fund FWF Grant. No. I 1452-N27 and by the DFG TR55, *Hadron Properties from Lattice QCD*. T. S. acknowledges the support of the U.S. Department of Energy Grant No. DE-FG02-03ER41260.

APPENDIX: CRITICAL μ'S AT STRONG COUPLING

In this appendix we derive the critical values of the chemical potential in the strong coupling limit which we use for comparing to our numerical data in Figs. 2 and 3.

For small values of J, the configurations that dominate the partition function Z of Eq. (12) have minimal values of all dual variables,

$$k_{x,\nu} = \bar{m}_{x,\nu} = 0 \quad \forall\ x,\nu \quad \text{and} \quad m_{x,1} = 0 \quad \forall\ x, \tag{A1}$$

except the temporal component of the flux variable, which assumes a constant value

$$m_{x,2} = r \quad \forall\ x, \tag{A2}$$

which amounts to r static particle worldlines on each temporal bond. From Eq. (14) it is clear that the resulting

particle density is $n = r$ (in lattice units). We restrict ourselves to positive μ and thus positive r for simplicity. These configurations obey the constraints in Eq. (12) and result in the partition functions

$$Z_r(J,\mu) = \left[\left(\frac{Je^{\mu}}{2}\right)^r \frac{\Gamma(1/2)}{\Gamma(r+3/2)}\right]^{N_s N_t}, \qquad \text{(A3)}$$

(where the factorials have canceled against Γ-factors from the beta function) or grand potential densities

$$\Omega_r(J,\mu) = -r\ln\left(\frac{Je^{\mu}}{2}\right) + \ln\Gamma(r+3/2), \qquad \text{(A4)}$$

up to an irrelevant additive constant. Certain values of r yield the smallest grand potential Ω_r depending on the values of μ and J. The neighboring values of r take over, when the corresponding Ω_r's become equal,

$$\Omega_r(J,\mu) = \Omega_{r-1}(J,\mu) \quad \text{for some } \mu = \mu_r, \qquad \text{(A5)}$$

which gives the following critical chemical potentials μ_r (in units of a),

$$e^{\mu_r} = \frac{2\,\Gamma(r+3/2)}{J\,\Gamma(r+1/2)}, \qquad \mu_r = \ln((2r+1)/J). \qquad \text{(A6)}$$

Note further that critical μ's inducing a density $n = r$ induce a charge $Q = rN_s$, and thus

$$\mu_{Q=rN_s} = \ln((2r+1)/J), \qquad \text{(A7)}$$

as used in Sec. III B.

[1] F. Bruckmann, C. Gattringer, T. Kloiber, and T. Sulejmanpasic, Grand Canonical Ensembles, Multiparticle Wave Functions, Scattering Data, and Lattice Field Theories, Phys. Rev. Lett. **115**, 231601 (2015).

[2] S. Chandrasekharan, A new computational approach to lattice quantum field theories, *Proc. Sci.*, LATTICE2008 (2008) 003 [arXiv:0810.2419].

[3] C. Gattringer, New developments for dual methods in lattice field theory at non-zero density, *Proc. Sci.*, LATTICE2013 (2014) 002 [arXiv:1401.7788].

[4] P. Rossi and U. Wolff, Lattice QCD with fermions at strong coupling: A dimer system, Nucl. Phys. **B248**, 105 (1984).

[5] F. Karsch and K. H. Mütter, Strong coupling QCD at finite baryon number density, Nucl. Phys. **B313**, 541 (1989).

[6] S. Sachdev, *Quantum Phase Transitions* (Cambridge University Press, Cambridge, England, 2011).

[7] F. Bruckmann and T. Sulejmanpasic, Nonlinear sigma models at nonzero chemical potential: Breaking up instantons and the phase diagram, Phys. Rev. D **90**, 105010 (2014).

[8] V. L. Berezinskii, Destruction of long range order in one-dimensional and two-dimensional systems having a continuous symmetry group. 1. Classical systems, Sov. Phys. JETP **32**, 493 (1971).

[9] J. M. Kosterlitz and D. J. Thouless, Ordering, metastability and phase transitions in two-dimensional systems, J. Phys. C **6**, 1181 (1973).

[10] D. Banerjee and S. Chandrasekharan, Finite size effects in the presence of a chemical potential: A study in the classical non-linear O(2) sigma-model, Phys. Rev. D **81**, 125007 (2010).

[11] K. Langfeld, Phase diagram of the quantum O(2)-model in $2+1$ dimensions, Phys. Rev. D **87**, 114504 (2013).

[12] H. Zou, Y. Liu, C.-Y. Lai, J. Unmuth-Yockey, L.-P. Yang, A. Bazavov, Z. Y. Xie, T. Xiang, S. Chandrasekharan, S.-W. Tsai, and Y. Meurice, Progress towards quantum simulating the classical O(2) model, Phys. Rev. A **90**, 063603 (2014).

[13] E. H. Lieb and W. Liniger, Exact analysis of an interacting Bose gas. 1. The general solution and the ground state, Phys. Rev. **130**, 1605 (1963).

[14] L. Tonks, The complete equation of state of one, two and three-dimensional gases of hard elastic spheres, Phys. Rev. **50**, 944 (1936).

[15] M. Girardeau, Relationship between systems of impenetrable bosons and fermions in one dimension, J. Math. Phys. (N.Y.) **1**, 516 (1960).

[16] C. N. Yang and C. P. Yang, Thermodynamics of one-dimensional system of bosons with repulsive delta function interaction, J. Math. Phys. (N.Y.) **10**, 1115 (1969).

[17] G. V. Dunne and M. Unsal, What is QFT? Resurgent trans-series, Lefschetz thimbles, and new exact saddles, *Proc. Sci.*, LATTICE2015 (2016) 010 [arXiv:1511.05977].

[18] G. V. Dunne and M. Ünsal, Resurgence and dynamics of O(N) and Grassmannian sigma models, J. High Energy Phys. 09 (2015) 199.

[19] G. V. Dunne and M. Ünsal, Resurgence and trans-series in quantum field theory: The CP(N-1) model, J. High Energy Phys. 11 (2012) 170.

[20] A. Cherman, D. Dorigoni, G. V. Dunne, and M. Ünsal, Resurgence in Quantum Field Theory: Nonperturbative Effects in the Principal Chiral Model, Phys. Rev. Lett. **112**, 021601 (2014).

[21] V. A. Fateev, V. A. Kazakov, and P. B. Wiegmann, Principal chiral field at large N, Nucl. Phys. **B424**, 505 (1994).

[22] P. Hasenfratz, M. Maggiore, and F. Niedermayer, The exact mass gap of the O(3) and O(4) nonlinear sigma models in $d = 2$, Phys. Lett. B **245**, 522 (1990).

[23] F. Bruckmann, C. Gattringer, T. Kloiber, and T. Sulejmanpasic, Dual lattice representations for O(N) and CP(N-1) models with a chemical potential, Phys. Lett. B **749**, 495 (2015); Erratum, Phys. Lett. B **751**, 595(E) (2015).

[24] C. Mudry, *Lecture Notes on Field Theory in Condensed Matter Physics* (World Scientific, Singapore, 2014).
[25] E. L. Pollock and D. M. Ceperley, Path-integral computation of superfluid densities, Phys. Rev. B **36**, 8343 (1987).
[26] S. H. Shenker and J. Tobochnik, Monte Carlo renormalization group analysis of the classical Heisenberg model in two-dimensions, Phys. Rev. B **22**, 4462 (1980).
[27] G. Fox, R. Gupta, O. Martin, and S. Otto, Monte Carlo estimates of the mass gap of the O(2) and O(3) spin models in $(1+1)$-dimensions, Nucl. Phys. **B205**, 188 (1982).
[28] B. Berg and M. Lüscher, Definition and statistical distributions of a topological number in the lattice O(3) sigma model, Nucl. Phys. **B190**, 412 (1981).
[29] N. Prokof'ev and B. Svistunov, Worm Algorithms for Classical Statistical Models, Phys. Rev. Lett. **87**, 160601 (2001).
[30] M. A. Cazalilla, R. Citro, T. Giamarchi, E. Orignac, and M. Rigol, One dimensional bosons: From condensed matter systems to ultracold gases, Rev. Mod. Phys. **83**, 1405 (2011).
[31] P. C. Hohenberg and B. I. Halperin, Theory of dynamic critical phenomena, Rev. Mod. Phys. **49**, 435 (1977).
[32] M. P. A. Fisher, P. B. Weichman, G. Grinstein, and D. S. Fisher, Boson localization and the superfluid-insulator transition, Phys. Rev. B **40**, 546 (1989).
[33] A. van Otterlo, K.-H. Wagenblast, R. Baltin, C. Bruder, R. Fazio, and G. Schön, Quantum phase transitions of interacting bosons and the supersolid phase, Phys. Rev. B **52**, 16176 (1995).
[34] H. Bethe, On the theory of metals. 1. Eigenvalues and eigenfunctions for the linear atomic chain, Z. Phys. **71**, 205 (1931).
[35] A. B. Zamolodchikov, Relativistic factorized S matrix in two-dimensions having O(N) isotopic symmetry, Nucl. Phys. **B133**, 525 (1978); JETP Lett. **26**, 457 (1977).
[36] B. Sutherland, *Beautiful Models, 70 Years of Exactly Solved Quantum Many-Body Problems* (World Scientific, Singapore, 2004).
[37] N. Levinson, On the uniqueness of the potential in a Schrodinger equation for a given asymptotic phase, Kgl. Danske Videnskab. Selskab, Mat.-fys. Medd. **25**, 9 (1949).